Plasma Electrodynamics and Applications

RLE Group
Plasma Electrodynamics Group

Academic Staff
Professor Abraham Bers

Visiting Scientists and Research Affiliates
Dr. Y. Peysson (TORE-SUPRA, CEA, Cadarache, France), Dr. M.M. Shoucri (IREQ, Canada), Dr. E.A. Williams (LLNL), Dr. A.B. Langdon (LLNL)

Graduate Students
Joan Decker and David J. Strozzi

Introduction

In continuation of the three projects, reported on in last year's Progress Report[1], the following have been accomplished:

1. Theoretical and computational work on current drive with electron Bernstein waves (EBW), in toroidally, magnetic confinement plasmas, has been completed. This is of importance to controlled fusion energy generation in magnetically confined plasmas (MCF) in general, and in particular for currently planned experiments on so-called spherical tokamaks - NSTX at the national facility at Princeton, and MAST in the U.K.. A detailed analysis of the possible means for generating such currents with externally driven EBW was part of the Ph.D. thesis of Mr. Joan Decker, completed in May 2005. Section 1 gives a summary of this work and its main conclusions.

2. In our studies of intense laser-plasma interactions, of importance to energy generation in inertial confinement fusion (ICF), we have continued our studies on the nonlinear evolution of stimulated Raman backscattering (SRBS) which may impose serious limitations on achieving fusion conditions with lasers. A new formulation and computer simulation of the interaction between plasma inhomogeneity and nonlinear effects due to particle trapping shows promise of understanding the saturation and control of SRBS. This work is part of the current Ph.D. thesis research of Mr. David Strozzi. Section 2 describes the progress in this research.

3. Based upon the high-frequency hydrodynamic description of waves, mentioned in last year's Progress Report, a new, self-consistent formulation of mode conversion in inhomogeneous plasmas has been derived. In particular, this has been applied to establishing the differential equations for the mode conversion excitation of EBW, in magnetically confined plasmas, from electromagnetic waves externally driven at the edge of such plasmas. This work has been recently presented and will be published in the proceedings of the conference[2].

[1] "Plasma Electrodynamics and Applications", Progress Report No. 146, MIT Research Laboratory of Electronics, Cambridge, 2004, Chapter 18.
[2] A. Bers and J. Decker, "Self-Consistent Formulation of EBW Excitation by Mode Conversion", to appear in Proceedings AIP of the 19-th Topical Confernce on Radio Frequency Power in Plasmas, Utah, June 2005

1. Electron Bernstein Wave Current Drive

Sponsor
Department of Eenergy (DOE) Grant No. DE-FG-91ER-54109 and EF-FG02-99ER-54521

Project Staff
J. Decker, Dr. Y. Peysson, and Professor A. Bers

The following is a summary and conclusions from a Ph. D. Thesis[3] submitted to the EECS Department in May 2005.

The calculation of current drive (CD) by EBWs in toroidal plasmas involves the solution of the fully-relativistic electron drift-kinetic equation with Fokker-Planck collisions and RF quasilinear diffusion. This equation, which accounts for particle orbit effects such as magnetic trapping and radial drifts, has been derived in a general formalism that is valid for an arbitrary axisymmetric magnetic geometry, and thus is adapted to the strongly shaped plasmas of spherical tokamaks.

The 4D drift-kinetic equation (2D in axisymmetric configuration space, 2D in gyro-averaged momentum space) is reduced to a set of two bounce-averaged 2D equations in momentum space. Solving these two partial integral-differential equations requires numerical techniques, and a new code named *DKE* has been developed for this purpose.

Spherical tokamaks and framework of EBWCD calculations

Spherical tokamaks are high- β plasma devices with a very small aspect ratio and thus a tight toroidal geometry. A particularity of high- β toroidal plasmas is the existence of a dip in the magnetic field profile, located off-axis on the outboard side of the plasma. Therefore, in a high- β plasma, it is possible to approch a harmonic resonance from either the LBF or the HBF region, with launching from the outboard side. In that case, LBF CD is located on the inboard side while HBF CD is located on the outboard side.

The EBWCD calculations presented in the thesis apply to the vicinity of the horizontal midplane, where the plasma is locally in a slab geometry so that the quasilinear operator is valid. This approximation requires that the EBW beam size be much larger than the wavelength, so that the wave is well defined in Fourier spectrum, but also much smaller than the length of poloidal field lines, so that the slab approximation applies. In that case, EBW damping and current drive can be calculated without ray-tracing techniques.

Low B-field ($n\omega_{ce} < \omega$) current drive

Since LBFCD occurs on the inboard side of the plasma, the LBFCD mechanism is the Fisch-Boozer effect, which results from the plasma collisional response to an asymmetric resistivity (in $p_{\parallel}$) created by asymmetric perpendicular heating of the distribution function.

- The CD efficiency decreases as the wave moves closer to the cyclotron harmonic resonance and the resonance curves move correspondingly closer to the bulk in momentum space, where resonant electrons are more collisional and carry less parallel momentum.

[3] J. Decker, "Electron Bertstein Wave Current Drive Modeling in Toroidal Plasma Confinement", Ph. D. thesis, EECS Department, M.I.T., May 2005.

- The large value of $\mathrm{Re}[k_\perp \rho_{Te}]$ in LBFCD results in confining the interaction to the vicinity of the $p_\perp = 0$ axis, which is favorable for Fisch-Boozer current drive because the resonance region is far from the trapped/passing boundary.
- The parallel component of the quasilinear diffusion - a relativistic effect - is directed towards the tail of the distribution in LBFCD, which is favorable for Fisch-Boozer current drive because more efficient direct parallel momentum is transmitted to the electrons.
- In LBFCD, the shift of power deposition due to relativisic effects is directed toward the resonance, which has a negative effect on CD since the CD efficiency is decreasing monotonically towards the resonance.
- As a consequence of these two relativistic effects, the normalized LBF driven current increases with $N_\parallel$ and remains rather independent of temperature.
- The effect of electron trapping is to reduce the CD efficiency, because the effect of collisional pitch-angle scattering is enhanced by trapped electrons.
- Quasilinear effects typically increase the LBF Fisch-Boozer CD efficiency.
- In HBFCD, the overlapping of harmonics is always deleterious because the mechanism for $n = 2$ HBFCD is dominated by the Fisch-Boozer effect on the inboard side of the plasma, where there are no trapped electrons. Because the HBF approach to the $n = 2$ resonance is on the opposite side in $p_\parallel$, current is driven in the opposite direction.

High B-field ($n\omega_{ce} < \omega$) current drive

- Since HBFCD occurs on the outboard side of the plasma and far off-axis, the HBFCD mechanism is the Ohkawa effect, which results from the asymmetric trapping (in $p_\parallel$) induced by the wave when barely-passing electrons are heated perpendicularly.
- The CD efficiency peaks at some distance from the resonance that corresponds to a situation where the diffusion coefficient in momentum space is located in the vicinity of the trapped-passing boundary, and thus wave-induced magnetic trapping is at its maximum. Farther from the resonance, the Fisch-Boozer effect counteracts the Ohkawa effect and the CD efficiency is reduced. Closer to the resonance, most of the power is coupled to the trapped electrons, which drive no current.
- Because of the smaller value of $\mathrm{Re}[k_\perp \rho_{Te}]$ in HFBCD, the interaction is located at larger $p_\perp$, which is favorable for Ohkawa current drive because the resonance region is close to the trapped/passing boundary, and large wave-induced trapping can occur.
- The parallel component of the quasilinear diffusion is directed towards the bulk of the distribution in HBFCD, which is favorable for Ohkawa current drive because wave-induced trapping is increased.
- In HBFCD, the shift of power deposition due to relativisic effects is directed away from the resonance. Its effect on CD depends on the relative positions of the CD efficiency and power deposition profiles.
- As a consequence of these two relativistic effects, the normalized HBF driven current increases with both $N_\parallel$ and the temperature.
- Optimizing OKCD requires a much larger fraction of trapped electrons than for ECCD, in order for the diffusion coefficient to be located close to the trapped/passing boundary in momentum space. Fortunately, STs typically have very large fractions of trapped particles, because of their small aspect ratio.
- In order to optimize OKCD, the fraction of trapped electrons - and thus the location of deposition - must be adjusted with quasilinear effects such that the peaks in the CD efficiency and power deposition profiles coincide.

- In HBFCD, the overlapping of harmonics is not necessarily deleterious because the mechanism for $n = 1$ LBFCD, far from the resonance, is dominated by the Fisch-Boozer effect, even on the outboard side of the plasma. Because the LBF approach to the $n = 1$ resonance is on the opposite side in $p_\parallel$, current is driven in the same direction.

Comparisons and conclusions

A comparison between LBF and HBF approaches is presented in the following table.

	LBF-EBWCD	**HBF-EBWCD**
Definition (vs. n^{th} harmonic)	$n\omega_{ce} < \omega$	$n\omega_{ce} > \omega$
Localization in high-β plasma	inboard side	outboard side
CD mechanism	Fisch-Boozer	Ohkawa
CD direction	opposite to $\mathbf{k}_\parallel$	opposite to $\mathbf{k}_\parallel$
Accessibility	restricted on midplane	very good on midplane
Accessible harmonics	only $n = 1$	any $n \geq 2$
Radial locations (in NSTX)	$0 \lesssim \rho \lesssim 0.6$	$0.6 \lesssim \rho \lesssim 1$
Deposition profile	very narrow	narrow to broad
Increasing $N_\parallel$	increases η	increases η
Increasing electron trapping	reduces η	increases η
Increasing temperature	little effect on η	increases η
$\Rightarrow$ effect of increased ρ	η decreases	η increases
Typical norm. CD efficiency	$\xi_{CD} \sim 0.67$	$\xi_{CD} \sim 0.37$
Typical CD efficiency in NSTX	$I/P \sim 0.1$ A/W	$I/P \sim 0.04$ A/W

For a given $N_\parallel$, LBF Fisch-Boozer CD and HBF Ohkawa CD are in the same direction, because the resonance curves in momentum space are located on opposite sides of the $p_\parallel = 0$ axis. This could be an important (and favorable) factor if part of the RF power happens to be absorbed in LBF approach on the inboard side and part of it in HBF approach on the outboard side.

The typical EBWCD efficiencies are significantly higher than ECCD efficiencies because the power - and the current - are deposited in the tail of the distribution function. For comparison, typical normalized ECCD efficiencies measured in comparable D3D plasmas are $\xi_{CD} \sim 0.3$ in the core and $\xi_{CD} \sim 0$ for $\rho \geq 0.4$. However, efficiencies are lower than for lower-hybrid current drive, because the diffusion is mostly in the perpendicular direction.

In general, a higher $N_{\parallel}$ leads to higher CD efficiencies for both Fisch-Boozer LBFCD and Ohkawa HBFCD. However, if $N_{\parallel}$ becomes too large, two harmonics can overlap. As for any current drive mechanism, an increased effective charge reduces both Fisch-Boozer LBFCD and Ohkawa HBFCD, because it tends to isotropize the distribution function.

Because of the particular magnetic geometry of high- β ST plasmas, LBFCD occurs on the inboard side and is possible only between first and second harmonic, and at radial locations $0 \lesssim \rho \lesssim 0.6$. Its efficiency generally decreases with ρ because of the larger fraction of trapped particles.

On the other side, the high- β ST plasma geometry limits HBFCD to the outboard side at locations $0.6 \lesssim \rho \lesssim 1$, where the mechanism is Ohkawa current drive. The variations of the CD efficiency with ρ depend upon many parameters, in particular the fraction of trapped electrons.

The radial width of the power deposition profile increases with the magnetic field variations scale length L_B and the Doppler broadening effect, proportional to $N_{\parallel}\beta_{Te}$. In HBFCD, it is possible to obtain very wide deposition profiles by driving current near the bottom of the dip in the magnetic field profile, where L_B becomes very large.

In conclusion, current can be efficiently driven by electron Bernstein waves in most radial locations in the plasma, provided the wave is launched near the midplane. The current drive mechanism is the Fisch-Boozer effect when the EC resonance is approached from a lower B -field region in the center of the plasma, and it is the Ohkawa effect when it is approached from a higher B -field region far off-axis on the outboard side.

2. Electron Trapping and Plasma Inhomogeneity in Stimulated Raman Scattering

Sponsor
Department of Energy

Project Staff
D. J. Strozzi, Dr. E. A. Williams (LLNL), Dr. A. B. Langdon (LLNL), Dr. M. M. Shoucri (IREQ), and Professor A. Bers

For inertial confinement fusion (ICF) to succeed, high-intensity lasers must propagate through large regions of underdense plasma. In ICF, radiation compresses a cold pellet of solid hydrogen to fusion conditions. Lasers irradiate the pellet (direct drive) or heat a hohlraum which radiates x-rays (indirect drive). One unwanted laser-plasma interaction is stimulated Raman scattering (SRS), where the pump laser decays to a light wave and an electron plasma wave. SRS takes energy out of the laser, and generates hot electrons via the plasma wave which can pre-heat the pellet.

We have studied kinetic effects, in particular electron trapping, in SRS. We developed an Eulerian kinetic code ELVIS to simulate Raman scattering. We focus on parameters of interest to underdense coronal plasmas filling indirect-drive ignition hohlraums, for instance those planned on the National Ignition Facility[4]. These plasmas have scale lengths of hundreds of microns, with electron temperatures of 1-6 keV and electron densities between 5% and 20% of the critical density ($n_c = \varepsilon_0 m_e \omega_0^2/e^2$ = 9.05 E27 m^{-3} for 351 nm light, as on NIF). The laser beams have averaged intensities of several 10^{14} W/cm^2 with speckles of intensities of several 10^{15} W/cm^2.

When the plasma is homogeneous, coupled-mode theory predicts for typical ICF hohlraum parameters that SRS is a convective instability with mild spatial gain. However, recent experiments[5] show reflectivities (around 10%) much larger than linear theory predicts. Not only is the absolute reflectivity level high, but it also shows a slight increase with $k\lambda_D$ of the Raman plasma wave ($\lambda_D = (\varepsilon_0 T_e/n_0 e^2)^{1/2}$ is the electron Debye length). Linear theory states the reflectivity should decrease dramatically with $k\lambda_D$, since Landau damping increases strongly as $k\lambda_D$ rises. Our simulations show that once electrons are trapped in the large-amplitude plasma wave, the reflected light greatly increases. Trapping flattens the electron distribution function near the plasma-wave phase velocity, and thus reduces Landau damping.

Plasma inhomogeneity, such as density gradients, lead to a spatial variation in the mode wavenumbers. Since SRS requires the wavenumbers to match, the variation restricts Raman to a region in space near the matching point. However, trapping nonlinearly shifts the plasma-wave frequency and wavenumber. Before studying how this affects the self-consistent Raman problem, we explore the plasma wave driven by a fixed external force (which represents, for instance, the beating of two imposed light waves). The wavenumber shift moves the resonance point as well as the driven amplitude. This shift depends on the direction of plasma wave propagation relative to the density gradient. In the SRS problem, the shift can either counteract or enhance the mismatch due to inhomogeneity. The shift may thus enhance SRS.

Coupled-Modes Theory

The coupled-mode equations (CMEs) describe the slow space-time evolution of the amplitudes of the three SRS modes. The basic PDEs that describe the waves involved in SRS are

$$\left(\partial_{tt} - c^2\nabla^2 + {\omega_p}^2\right)\vec{V}_0 = -{\omega_p}^2 \frac{n_2}{n_B}\vec{V}_1 \tag{1}$$

[4] J. Lindl *et al.*, *Phys. Plasmas* **11**, pp. 339-491 (2004).
[5] J. C. Fernandez *et al*., *Phys. Plasmas* **7**, pp. 3743-3750 (2000).

$$\left(\partial_{tt} - c^2\nabla^2 + {\omega_p}^2\right)\vec{V}_1 = -{\omega_p}^2 \frac{n_2}{n_B}\vec{V}_0 \tag{2}$$

$$\left(\partial_t + \vec{v}\cdot\nabla - e\vec{E}\cdot\nabla_p\right)f_e = m_e\left(\nabla_p f_e\right)\cdot\nabla\left(\vec{V}_0\cdot\vec{V}_1\right) \tag{3}$$

Subscripts 0, 1, and 2 refer to the pump, scattered, and plasma wave, respectively. $\vec{V}_i$ is the electron oscillation in light wave i. f_e is the electron distribution and n_2 the plasma-wave density fluctuation. The first two equations describe the evolution of the pump and scattered light waves due to the Raman process, while the third is the Vlasov equation for the plasma wave with coupling to the light waves. Throughout this report we relate momentum and velocity nonrelativistically: $p_e = m_e v_e$. The left-hand sides are the wave operators that give the natural modes (light and plasma waves) in the absence of coupling. The right-hand sides are the parametric coupling. In the first two equations, each light wave is driven by the current density perturbation from n_2 and the other light wave. The plasma wave is driven by the vxB force from the beating of the two light waves. ${\omega_p}^2 = (n_B e^2/\varepsilon_0 m_e)$ defines the plasma frequency, and n_B is the background density, which may vary in space. We shall use ω_{p0} and λ_{D0} with subscript zeros to denote the plasma frequency and Debye length evaluated at a reference density n_0 (as opposed to the spatially-varying ω_p and λ_D computed with the local density).

We represent the electric field for each mode as a slowly-varying (with respect to ω_i and k_i) amplitude a_i times a carrier wave:

$$\vec{E}_i \propto \vec{e}_i a_i \exp i\left(\vec{k}_i\cdot x - \omega_i t\right) + c.c. \qquad \left|\partial_x a_i\right| << \left|\vec{k}_i a_i\right|, \qquad \left|\partial_t a_i\right| << \left|\omega_i a_i\right| \tag{4}$$

a_i is the action amplitude of mode i (we omit the constant relating action amplitude to electric field). The action density N_i (=energy density / frequency) of mode i is $N_i = a_i a_i^*$. The coupling maximizes when the phase of each mode and its drive match. This gives the resonance or matching conditions $\omega_0 = \omega_1 + \omega_2$, $\vec{k}_0 = \vec{k}_1 + \vec{k}_2$. These also represent energy and momentum conservation, respectively. The k's vary with x in an inhomogeneous plasma. $\vec{k}_0$ and $\vec{k}_1$ satisfy the local light-wave dispersion relation: $\left|\vec{k}_i\right| = (1/c)\left({\omega_i}^2 - {\omega_p}^2\right)^{1/2}$. $\vec{k}_2(x)$ is the beat mode of the light waves; it is the real part of a natural plasma wave only at the resonance point.

SRS maximizes when the coupling in the kinetic equation is largest, that is, when $\vec{V}_0 \| \vec{V}_1 \| \hat{y}$. This restricts the k's to the x-z plane. Since the focused regions of high laser intensity are much narrower than they are long in the direction $\vec{k}_0$, SRS has a much longer amplifying region for $\vec{k}_0 \| \vec{k}_1 \| \vec{k}_2$. We thus adopt the 1-D geometry where all k's point in the x direction. The resulting coupled-modes equations are

$$\left(\partial_t + v_{g0}\partial_x + \nu_0\right)a_0 = K a_1 a_2 \tag{5}$$

$$\left(\partial_t + v_{g1}\partial_x + \nu_1\right)a_1 = -K a_1 a_2^* \tag{6}$$

$$\varepsilon\left(\omega_2 + i\partial_t, k_2 - i\partial_x\right)a_2 = -2i\frac{\omega_2}{{\omega_{p0}}^2}\chi K a_0 a_1^* \tag{7}$$

We have added collisional light-wave damping ν_0, ν_1. v_{gi} is the group velocity of mode i and K is the SRS coupling constant. χ and $\varepsilon = 1+\chi$ are the kinetic plasma-wave susceptibility and permittivity, respectively. Since the coupling weakly modifies the natural mode (that is, growth rates are much less than natural frequencies), we use the linear χ. ε is an operator that includes the slow amplitude variation via ∂_x and ∂_t. It also depends nonlinearly on a_2 to include trapping effects. For weak nonlinearity we treat the shift perturbatively: $\varepsilon = \varepsilon_l + \delta\varepsilon$ where ε_l is the linear permittivity and $\delta\varepsilon$ a nonlinear correction.

The usual coupled-modes plasma wave equation results from expanding ε for slow a_2 variation:

$$\varepsilon(\omega_2 + i\partial_t, k_2 - i\partial_x) \approx \varepsilon(\omega_2, k_2) + i\frac{\partial \varepsilon}{\partial \omega_2}\partial_t - i\frac{\partial \varepsilon}{\partial k_2}\partial_x \tag{8}$$

For a homogeneous plasma, with k_2 the real k for a natural mode, ε reflects damping and the nonlinear shift. Neglecting nonlinearity and evaluating ε_l and χ in the fluid limit gives the CMEs:

$$D_0 a_0 = K a_1 a_2 \qquad D_i \equiv \partial_t + v_{gi}\partial_x + \nu_i \tag{9}$$

$$D_1 a_1 = -K a_1 a_2^* \qquad K \equiv \frac{\omega_{p0}^2}{\sqrt{8 n_0 m_e}} \frac{k_2}{\sqrt{\omega_0 \omega_1 \omega_2}} \tag{10}$$

$$D_2 a_2 = -K a_0 a_1^* \tag{11}$$

An instability analysis of the CMEs for fixed a_0 (no pump depletion) shows SRS is unstable when the undamped growthrate $\gamma_0 \equiv K a_0 > (\nu_1 \nu_2)^{1/2}$. SRS is a convective instability unless the more stringent absolute instability condition is met:

$$\gamma_0 > \frac{1}{2}\sqrt{|v_{g1} v_{g2}|}\left(\frac{\nu_1}{|v_{g1}|} + \frac{\nu_2}{|v_{g2}|}\right) \tag{12}$$

In typical ICF hohlraum conditions mentioned above, the laser intensity is high enough, and light-wave collisional damping weak enough, that the laser is above the SRS instability threshold but below the absolute threshold. If the Landau damping of the plasma wave were eliminated, for instance by trapping, the residual collisional damping provides a very weak absolute threshold; SRS would then become absolutely unstable and would reach very large levels.

When SRS is not absolutely unstable, it approaches a temporal steady state. We set $\partial_t = 0$ in the CMEs Eqs. (9-11) and solve for the spatial amplitude gain rate α. For backscatter,

$$\alpha = \frac{1}{2}(\sigma_2 - \sigma_1) - \left(-\alpha_0^2 + \frac{1}{4}(\sigma_1 + \sigma_2)^2\right)^{1/2} \qquad \alpha_0 = \frac{\gamma_0}{\sqrt{|v_{g1} v_{g2}|}}$$

$\sigma_{1,2}$ are the positive spatial damping rates of modes 1 and 2. Figure 1 shows α as a function of electron density and temperature. The pump light has intensity I_0 = 2E15 W/cm^2 and wavelength λ_0 = 351 nm. No collisional damping was included, although the results are nearly identical if it is. Ignition hohlraums typically have plasmas toward the low-density, high-temperature quadrant. For instance, n_0/n_c = 0.1 and T_e = 3 keV gives a gain length α^{-1} = 52.6 μm. Even over a L = 0.5 mm homogeneous gain region the power gain exponent is G = (2 α L) = 19, which is negligible (typically G > 30 is considered necessary for amplifying thermal noise to important levels in ICF).

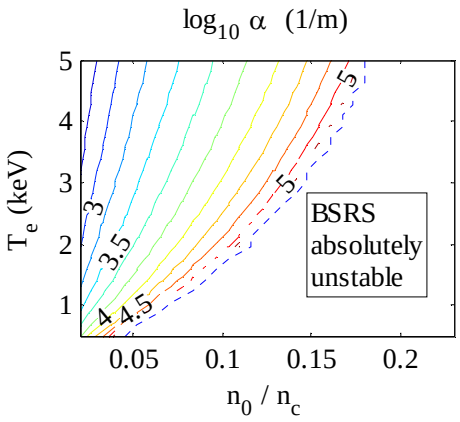

Figure 1: Spatial gain rate alpha vs. electron density / critical density and electron temperature.

Next, consider an inhomogeneous plasma. The instability is, in principle, always convective for a linear gradient. We consider the steady state and neglect light-wave damping. In addition, it is usually a good approximation to neglect plasma-wave advection as being weak compared to damping or mismatch. This approximation is called the strong damping limit and entails setting $\partial_x = 0$ in the permittivity operator. The resulting CMEs are

$$v_{g0}\partial_x a_0 = K a_1 a_2 \tag{13}$$

$$v_{g1}\partial_x a_1 = -K a_1 a_2^{*} \tag{14}$$

$$\varepsilon(\omega_2, k_2) a_2 = -2i \frac{\omega_2}{\omega_{p0}^2} \chi K a_0 a_1^{*} \tag{15}$$

Here, ε includes damping, mismatch from inhomogeneity, and the nonlinear shift. Neglecting the shift, we can solve the system analytically, including pump depletion. We consider backscatter, where the pump mode 0 (scattered mode 1) wave enters from the left edge x_L (right edge x_R) with a known intensity and propagates to the right (left). Let Z_0, Z_1 be the normalized light-wave action fluxes:

$$Z_0 \equiv \frac{N_{0L}}{N_0} \qquad Z_1 \equiv -\frac{v_{g1}}{v_{g0}} \frac{N_1}{N_{0L}} \tag{16}$$

The steady-state solution satisfies the Manley-Rowe relation $Z_0 - Z_1 = \text{const.}$, and

$$Z_1 = \hat{Z}\left[\left(1 + \hat{Z}/Z_{1R}\right) e^{-\hat{Z}G(x)} - 1\right]^{-1} \qquad \hat{Z} \equiv 1 - Z_{1L} \tag{17}$$

$$G(x) \equiv -4 \frac{\gamma_0^2}{v_{g1}} \frac{\omega_2}{\omega_{p0}^2} \int_x^{x_R} dx' g_I(x') \qquad g_I \equiv \mathrm{Im}\left[\frac{\chi}{\varepsilon}\right] \tag{18}$$

In the limit of weak scattering (no pump depletion, $Z_0 \approx$ const), $Z_1 = Z_{1R} \exp G(x)$, that is, we have exponential growth with a spatially-varying gain exponent.

ELVIS code

ELVIS[6] solves the 1-D Vlasov-Maxwell system using the algorithm developed by Ghizzo et al.[7] The geometry, along with a sample density and Krook damping rate, are given in Fig. 2. The equations are:

$$\left(\partial_t + v_x\partial_x + eZ_s\left(E_x + v_{ys}B_z\right)\partial_{p_x}\right)f_s = -\nu_{Ks}(x)\left(f_s - n_s\hat{f}_{0Ks}\right) \tag{19}$$

$$\partial_x E_x = \rho \qquad \rho = e\sum_s Z_s n_s \tag{20}$$

$$E^{\pm} = E_y \pm cB_z \tag{21}$$

$$\left(\partial_t \pm c\partial_x\right)E^{\pm} = -\varepsilon_0^{-1}J_y \qquad J_y = e\sum_s Z_s n_s v_{ys} \tag{22}$$

$$m_s\partial_t v_{ys} = eZ_s E_y \tag{23}$$

ELVIS handles an arbitrary number of kinetic species, labeled by *s*, but usually we just run with mobile electrons and keep the ions fixed. Z_s and m_s are the species charge state and mass. The right-hand side of the kinetic equation is a Krook relaxation operator. It is intended to represent the loss of particles out of the narrow laser beam due to their transverse motion (sideloss), rather than collisions. We let the relaxation rate $\nu_{Ks}(x)$ vary with x. Frequently we run with a large ν_{Ks} near the edges of the density profile, to reduce edge fluctuations and prevent plasma wave reflection. In the transverse y direction, each species is a cold collisionless fluid. The code is Eulerian, as opposed to particle-in-cell, because we solve for f_s on a fixed grid in (x,p) phase space. We advance f_s using Strang operator splitting and use cubic splines for interpolation.

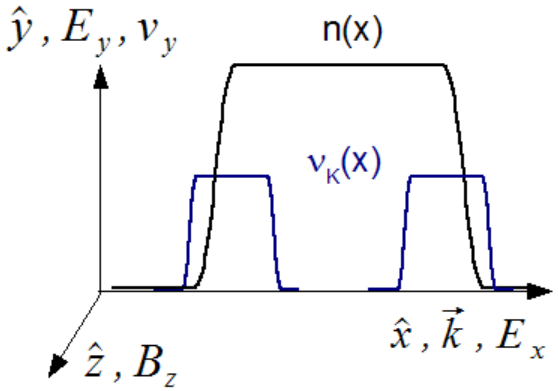

Figure 2: ELVIS 1-D Geometry with sample density and Krook profile

ELVIS has several modes of operation to study problems besides SRS. It can solve the electrostatic equations with no transverse electromagnetic fields ($E^{\pm}$). Also, it allows for an external force in the x direction, which is not self-consistent with the plasma charges and currents. This is useful for studying the plasma response to an imposed force.

Homogeneous plasma simulation results

ELVIS simulations have shown that homogeneous plasmas give reflectivities much higher than linear coupled-modes theory. We present results for a plasma with n_e = 0.1n_c, T_e = 3 keV, and pump characteristics used for Fig. 1 (I_0 = 2E15 W/cm^2, λ_0 = 351 nm). Eulerian kinetic codes do not have the

[6] D. J. Strozzi, M. M. Shoucri, and A. Bers. *Comp. Phys. Comm.* **164**, pp. 156-159 (2004); RLE Progress Report 2003-2004, section 18.5.
[7] A. Ghizzo et al., *J. Comput. Phys.* **90**, pp. 431-457 (1990).

high noise levels of PIC codes, which arise from single-particle discreteness effects. Therefore, the ELVIS simulation has very low fluctuations for SRS to grow from. To remedy this we introduce a seed light wave with I_1 = 2E10 W/cm^2 (= 1E-5 I_0) and λ_1 = 574 nm (this λ_1 gives the largest linear growthrate). The pump and seed lasers impinge on the plasma from the left and right, respectively. SRS is a convective instability according to linear coupled-modes theory, with a homogeneous gain rate α = 0.0190 / μm, or a gain length α^{-1} = 52.6 μm. The density profile is like that in Fig. 2, with a flattop, Krook-free region of length L = 75 μm. The linear reflectivity estimate is R = I_{1L}/I_{0L} = 1.43E-4.

We show the time evolution of the simulation reflectivity in Fig. 3. It clearly reaches levels well above linear theory. The reflectivity is bursty in time, and no steady state is reached. Figures 4 (left) displays a contour plot of the electron distribution f_e at a time shortly before the first burst of large reflectivity. Vortices at the plasma-wave phase velocity v_{p2} = 0.264c due to electron trapping are clearly present. The space-averaged f_e presented in Fig. 4 (right) reveals f_e is flattened in the neighborhood of v_{p2}. Since the Landau damping rate is proportional to $df_e/dv(v=v_{p2})$, a flattened distribution gives greatly reduced Landau damping. A similar enhancement in SRS has been shown in reduced-PIC simulations[8]. Although the simulation has no collisional damping, we do not think it significantly limits the reflectivity. In the absence of collisions, the absolute instability threshold is several orders of magnitude lower than the pump intensity. With or without collisions, SRS grows until some nonlinearity (e.g., pump depletion, the nonlinear frequency shift, or the trapped particle instability[9]) saturates it.

The physics of electron trapping is as follows. In the wave's frame of reference, electrons see a sinusoidal potential, and their equation of motion is that of a nonlinear pendulum. Particles with lab-frame speeds far enough from v_{p2} are "passing:" their speed changes slightly as they go over the potential hills and valleys, but they never change direction. Particles moving near v_{p2}, however, oscillate back and forth in the potential well and are called "trapped."

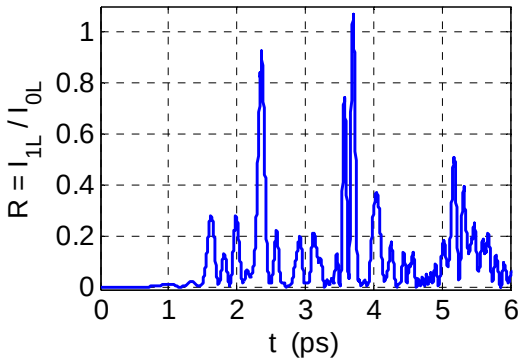

Figure 3: Reflectivity (ratio of light-wave intensities) vs. time for homogeneous plasma.

[8] H. X. Vu, D. F. DuBois and B. Bezzerides, *Phys. Rev. Lett.* **86**, pp. 4306-4309 (2001).
[9] S. Brunner and E. J. Valeo, *Phys. Rev. Lett.* **93**, p. 145003 (2004).

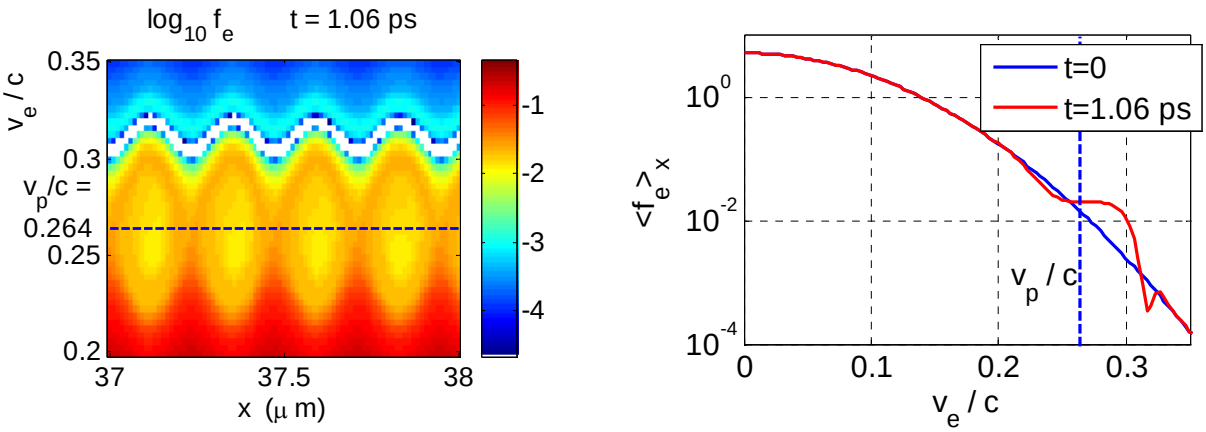

Figure 4: Left: contour plot of electron distribution f_e (white: f_e below cutoff value). Right: space-averaged f_e.

Nonlinear shifts in driven plasma waves

As homogeneous simulations and some experiments indicate, linear theory can fail very badly to predict Raman scattering. However, many effects neglected in these simulations may reduce SRS to much lower levels. Our recent work focuses on the role of plasma inhomogeneity in particular, and how this interacts with the nonlinear change in the plasma permittivity due to trapping. Following the standard WKB picture, spatial inhomogeneity does not affect the mode frequencies but causes the wavenumbers to vary over distances much longer than the wavelengths. As stated above, k_0 and k_1 are the spatially-varying natural k's for fixed ω's, while $k_2 = k_0 - k_1$ is the beat wavenumber. For weak nonlinear shift, we obtain from Eq. (15) an envelope equation for a_2:

$$\left(i\kappa(x) + \sigma_{2l} - i\delta k_2\right)a_2 = -2\frac{\omega_2}{\omega_{p0}^{\ 2}}\frac{\chi}{\varepsilon_l'}Ka_0a_1^{\ *} \tag{24}$$

$k_{2l} = k_{2lr} + i\sigma_{2l}$ is the complex, linear, spatially-varying natural mode corresponding to ω_2: $\varepsilon_l(k_{2l},\omega_2) = 0$. $\varepsilon_l' = \partial\varepsilon_l/\partial k_{2l}$. σ_{2l} is the linear spatial damping rate. $\kappa = k_2 - k_{2lr} \approx \kappa' x$ is the wavenumber mismatch (we expand about the resonance point x=0 where $k_2 = k_{2lr}$).

Before treating the full SRS problem, imagine the simpler case where the light waves have fixed, uniform amplitudes and beat to drive a plasma response. Let δn_e be the resulting external density perturbation amplitude (not self-consistent with the plasma-wave density fluctuation). The total density perturbation δn from both the external force δn_e and self-consistent plasma response δn_{sc} is $\delta n = \delta n_e + \delta n_{sc}$. The driven plasma wave satisfies an equation like Eq. (15) with δn_e replacing the light waves ($a_0a_1^{\ *}$) on the right-hand side. Neglecting advection (that is, assuming the strong damping limit applies) but including nonlinearity, the driven plasma-wave density amplitude is

$$\frac{\delta n_{sc}}{n_0} = \left(1 - \frac{1}{\varepsilon_l(k_2) + \delta\varepsilon}\right)\frac{\delta n_e}{n_0} \tag{25}$$

As expected, the response is large when the beat mode k_2 is almost a normal mode, and ε_l is small.

Figure 5 shows the rms density fluctuation for a series of electrostatic ELVIS runs. Each plot shows the numerical results with the driver propagating toward high density (solid blue curves) and low density (dotted green curves), as well as the analytic estimate from Eq. (25) (dashed red curves) without nonlinearity ($\delta\varepsilon = 0$). The plasma wave approaches a steady state in time. The numerical peaks are shifted from the analytic peaks in the direction of plasma wave propagation. This likely arises from the

slow ∂_x advective term which we neglect in the strong damping limit. The numerical peaks also have a larger amplitude than the analytic peaks, which is probably due to the nonlinear damping reduction.

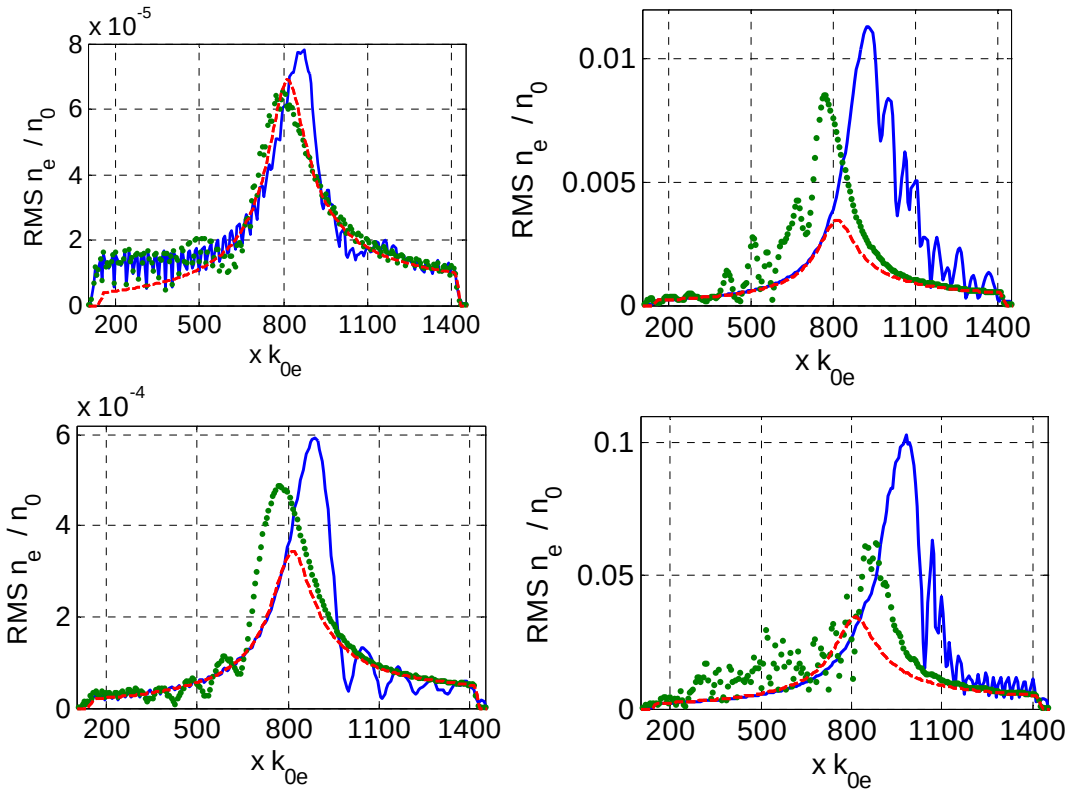

Figure 5: Density fluctuation from ELVIS simulations with plasma wave propagating to higher density (solid blue), ELVIS simulations with plasma wave propagating to lower density (dotted green) and strong damping limit Eq. (25) with $\delta\varepsilon = 0$ (dashed red). All runs have $\omega_2 = 1.18\omega_{p0}$, $|k_2\lambda_{D0}| = 0.313$. $\delta n_e / n_0$ = 4E-6 (top left), 2E-5 (bottom left), 2E-4 (top right), 2E-3 (bottom right). Profiles taken at a time after they settled into a steady state.

We are currently investigating what the implied nonlinear k shift in these simulations is, and how that compares with analytic estimates. This will shed light on simulations of Raman scattering in inhomogeneous plasmas which we are performing.